Pharmaceutical Research, Vol. 27, No. 2, February 2010 (© 2009)
DOI: 10.1007/s11095-009-0010-4

Research Paper

Hydrodynamic and Species Transfer Simulations in the USP 4 Dissolution Apparatus: Considerations for Dissolution in a Low Velocity Pulsing Flow

Deirdre M. D'Arcy,[1,3] Bo Liu,[1] Geoff Bradley,[2] Anne Marie Healy,[1] and Owen I. Corrigan[1]

Received July 14, 2009; accepted November 3, 2009; published online December 10, 2009

Purpose. To simulate the hydrodynamics in the flow-through (USP 4) dissolution apparatus and investigate the effects of hydrodynamics on mass transfer in a low velocity pulsing flow.
Methods. Computational fluid dynamics (CFD) was used to simulate the hydrodynamics and mass transfer in pulsing flow. Experimental flow visualisation was used to qualitatively confirm simulated hydrodynamic and mass transfer features. The experimental dissolution rate at 8 ml min^{-1} (22.6 mm flow-through cell) was compared to the experimental dissolution rate in a free convection system.
Results. Simulations revealed periods of low velocity at all flow rates, evidence of boundary layer separation, and, at higher flow rates, residual fluid motion during zero inlet velocity periods. The simulated diffusion boundary layer thickness varied in certain regions over the course of the pulse. The experimental dissolution rate in the free convection system was faster than that at 8 ml min^{-1} in the flow-through apparatus.
Conclusions. A low velocity pulsing flow running counter to gravity inhibited the experimental dissolution rate compared to that in a free convection system. From the CFD simulations generated, simulation of both hydrodynamics and species transfer is recommended to characterise the influence of hydrodynamics on dissolution in a low velocity pulsing flow.

KEY WORDS: computational fluid dynamics (CFD); dissolution; flow-through dissolution apparatus (USP apparatus 4); flow visualisation; hydrodynamics.

INTRODUCTION

The flow-through dissolution apparatus offers several advantages over the paddle and basket apparatuses. These include the ability to maintain sink conditions due to the continuous introduction of dissolution medium to the dissolution cell in an open system and the ease with which the composition and pH of the dissolution medium can be changed over the course of a dissolution test. Dissolution rates from a flow-through apparatus have previously been investigated in relation to flow rates (1–9). Comparisons have also been made between dissolution rates in the paddle apparatus and the flow-through apparatus (3,7,8,10). Suggested flow rates in the flow-through dissolution apparatus (USP apparatus 4 (Flow-Through Cell)) are 4 to 16 ml min^{-1} (11), although higher flow rates can be, and have been, used (4).

Electronic supplementary material The online version of this article (doi:10.1007/s11095-009-0010-4) contains supplementary material, which is available to authorized users.

[1] School of Pharmacy and Pharmaceutical Sciences, Trinity College Dublin, Dublin 2, Ireland.
[2] Trinity Centre for High Performance Computing, Trinity College Dublin, Dublin 2, Ireland.
[3] To whom correspondence should be addressed. (e-mail: ddarcy@tcd.ie)

ABBREVIATIONS: CFD, Computational Fluid Dynamics; min, minute; NaOH, sodium hydroxide; ppm, parts per million; rpm, revolutions per minute; s, seconds; USP, United States Pharmacopeia.

An estimate of average flow velocity over time at 16 ml min^{-1} through the smaller 12 mm diameter cell results in an average fluid velocity value of $2.4\times10^{-3}ms^{-1}$. The velocity will, obviously, be intermittently higher due to the pulsing nature of the flow through the cell. A similar estimate of 8 ml min^{-1} through the 22.6 mm diameter cell results in an average fluid velocity of approximately $3.3\times10^{-4}ms^{-1}$. In each case, fluid velocity values are much lower than those present in the paddle and basket apparatuses. Agitation rates of 50–75 or 50–100 rpm in the paddle apparatus and 50–100 or 100–150 rpm in the basket apparatus have been suggested as being suitable for routine dissolution testing and bioavailability and bioequivalence studies (12,13). Computational fluid dynamics (CFD) has been used to simulate hydrodynamics in both the paddle and basket apparatuses (14–20). Simulations at 50 rpm in both apparatuses have resulted in simulated velocity values ranging from almost zero to maximum values of 4.9×10^{-2} to $6.7\times10^{-2}ms^{-1}$ in the paddle apparatus (at 1 mm distance from a 13 mm diameter compact located at the centre of the vessel base) and $2.6\times10^{-2}ms^{-1}$ in the basket apparatus (relative to a compact in the basket of the apparatus) (18). The maximum fluid velocities in the flow-through apparatus at standard operating conditions are, therefore, expected to be considerably lower than those found in the paddle or basket apparatuses.

CFD fluid flow simulations of the paddle and basket apparatuses have also provided an insight into hydrodynamic variation within these apparatuses. This has assisted in the

interpretation of variation in dissolution rates at a constant agitation rate (17–20). It has been suggested that characterisation of the hydrodynamics within a dissolution apparatus is essential to determine the appropriateness of the application of general convective-diffusion theory, as described by Levich (21), in interpretation of dissolution test results (22). With respect to characterisation of flow in the flow-through apparatus, there has recently been a thorough analysis of the approach to classification of flow regimes within the flow-through apparatus from a fluid mechanics point of view (23). There has also been a comprehensive examination of simulated flow over the course of the pulse-inflow (pump discharge) in the 22.6 mm diameter cell in several different cell configurations: "no beads," "open column" and "packed column" operational modes (24). The flow-through apparatus provides a pulsing flow at 120 (± 10) pulses per minute (11); therefore, the hydrodynamics within the cell are time-dependent and, due to the nature of the pulse, will include periods of very low, or zero, velocity, in particular during the zero-inflow (pump suction) phase. As a result, it can be envisaged that the dissolution rate within the cell may also vary over the course of each pulse. Characterisation of the pulsing flow within the flow-through apparatus over the course of the whole pulse (pump suction and pump discharge) is therefore vital in determining the appropriateness of the pulsing flow field in dissolution testing. Furthermore, it was recognised that experimental research is required to optimally interpret the theoretical and simulated results presented (24). The current work focuses on the "packed column" operational mode, that is, with the conical part of the dissolution cell filled with glass beads. CFD hydrodynamic simulations of the entire pulse (pump suction and discharge periods) in both the 12 and 22.6 mm diameter cells are presented at several flow rates. Experimental flow visualisation studies were used to qualitatively support the CFD hydrodynamic simulations generated.

It has been highlighted that the pulsing nature of the flow in the flow-through apparatus promotes cycles of continuously changing dissolution kinetics (25) and that an elimination of the pulsing flow reduces the possibility of random flow movements. Furthermore, under low velocity conditions, the contribution from natural convection at the dissolving surface to the dissolution rate may be significant (5,18). Natural convection arises from the effect of gravity on the density difference between the concentrated solution at the dissolving interface and the surrounding bulk dissolution medium. In the flow-through cell, the upward-moving pulsing flow is running counter to any downward-flowing natural convection in the low velocity flow field. Investigation of the variation, with time, of both the hydrodynamics and the diffusion boundary layer at the dissolving surface over the course of the pulsing flow is essential to interpreting any potential interaction between natural and forced convection. In the current work, both flow visualisation studies and simulations of mass transfer, or "species transfer," from the dissolving surface are used to characterise the local hydrodynamics at the dissolving surface and the diffusion boundary layer under relatively "fast" flow conditions (12 mm diameter cell at a flow rate of 17 ml min^{-1}).

Comparisons of the effect of the pulsing flow on dissolution with dissolution in a free convection system are of interest, as in the *in vivo* situation, a dosage form may be subject to low velocity fluid flow and periods of time when a dosage form is essentially static. Furthermore, it may be located in inhomogenously distributed "pockets" of intestinal fluid (26). Experimental dissolution rates from a vertically orientated planar surface in a free convection (static fluid) system and a very low velocity pulsing flow field (8 ml min^{-1} in the larger 22.6 mm diameter cell) can be investigated using CFD simulations of this low velocity flow field. The dissolution rates can be compared and interpreted using the CFD simulation to give an insight into the potential for both natural convection and boundary layer separation to influence the diffusion boundary layer on a vertical surface and, thus, the dissolution rate under these conditions. Dissolution using benzoic acid has been generated in the paddle and basket apparatuses (18,20), and the resulting dissolution rates interpreted using CFD, which suggested that under low velocity conditions natural convection may contribute significantly to the dissolution rate (18). Therefore, in the current work, the model drug used to investigate dissolution under very low velocity pulsing flow and natural convection conditions was benzoic acid.

The aims of the current work are as follows:

1. To simulate, using CFD, the hydrodynamics within the cylindrical portion of the flow-through dissolution cell over the course of the whole pulse, focussing on flow in the region of a compact at the location of the tablet holder, and to compare results obtained with experimental flow visualisation results to support the simulation methodology employed. The whole pulse comprises pump suction and discharge. Hydrodynamics at several flow rates were studied.
2. To extend the model to include a mass transfer simulation, and to simulate the effect of pulsing flow on the solute concentration gradient in the region of the compact surface.
3. To determine the experimental dissolution rate of a vertically-orientated planar surface under low velocity conditions in the flow-through apparatus, and to interpret this dissolution rate using both i) a CFD simulation of these flow conditions and ii) the dissolution rate under conditions of no forced convection (natural convection), to investigate the interaction of forced and natural convection in conditions of low velocity pulsing flow.

MATERIALS AND METHODS

Computational Methods

CFD Simulation

The method used in carrying out the CFD simulations was as previously described (27). The CFD package Fluent™ (version 6.1.18) was used to simulate the hydrodynamics within the cell of the flow-through apparatus. The geometry used was constructed in the pre-processing package, Gambit™ (version 2.0.4 (Fluent (Ansys) Inc., N.H., U.S.A.)), and the fluid flow field was solved using the Fluent™ solver (Fluent (Ansys) Inc., N.H., U.S.A.).

A geometrically periodic model was constructed, consisting of one quarter of the 12 mm diameter cell, from the point at the top of the glass beads (the cylindrical part) to the outflow at the top of the cell (Fig. 1). One quarter of a disc of the same dimensions and orientation as the compact used in the flow visualisation studies was included in the model of the cell. The flow field was solved using symmetry conditions at the faces used to define the edge of the quarter flow field. For the 22.6 mm diameter cell, the full cylinder from the top of the glass beads to the filter at the top of the cell was constructed. A laminar time-dependent solver was used to find a solution to the fluid flow field. The time taken for one pulse (0.5 s) was divided into 50 time-steps, and a solution to the flow field at each of these time-steps was determined. The solution was considered converged when the residuals of continuity and velocity in x, y and z directions ceased to change on further iteration through the flow field. The residuals decreased to levels of 10^{-5} to 10^{-18} depending on the time-point of the pulse being simulated.

The flow to the cell is provided by a piston pump. As the liquid enters the cell, there is a half-sine-wave flow profile (caused by upward movement of the piston, also described as "pump discharge"). During the downward movement of the piston (also described as "pump suction"), the pump is drawing medium from the reservoir into the pump, with no discharge out of the pump. As a result, this part of the cell inlet flow profile is flat. Therefore, for the CFD simulations, the inlet flow profile over one pulse was described by a half-sine-wave for half of the pulse and a flat profile, with no flow, for the second half of the pulse.

A user-defined function (UDF) describing a time-dependent boundary condition was employed to define the flow at the inlet. This inlet velocity was assumed constant across the diameter of the inlet at any point in time. The Reynolds number in the test section of the cell (the region where the dosage form is most often located, in this case the region of the tablet holder), at both average and peak velocity values of the flow profile, supports the assertion of a laminar flow regime at the flow rates investigated (23). Therefore, a laminar, uniform flow was introduced at the inlet, with the rate of flow defined at each time-step to provide the appropriate inlet flow profile over the time-course of one pulse. The time-dependent boundary condition incorporated an equation of the form

$$\text{Velocity} = (\text{Volumetric flow rate} \,/\, \text{cell cross-sectional area}) \times \pi \times \sin(4\pi t) \quad (1)$$

where t is the time-point of the flow profile from 0 to 0.25 s. For $0.26\ \text{s} \le t \le 0.5$ s, the velocity of the inlet flow profile is defined as zero. The flow profile generated from this velocity inflow equation has been shown to match the actual flow profile metered during discharge from the piston pump (23).

A previous comparison of CFD simulations of flow using the porous zone approach, to replicate the beads effect, and of flow in a cell without the glass beads, lead to the conclusion that the presence of the beads made little difference to the hydrodynamics around the tablet while in the tablet holder (24). Therefore, the fluid inlet in the current work was defined as the base of the cylindrical part of the cell, i.e. above the conical part. It should be emphasised that this inlet boundary condition does not, therefore, simulate flow through the glass beads, which would involve considerable computational expense. Rather, this inlet boundary condition is used to generate a realistic simulation of flow conditions around the compact in the tablet holder.

The shape of the inlet flow profile is illustrated in Fig. 2. Flow rates of 5, 17 and 33 ml min^{-1} were simulated in the 12 mm diameter cell, and 8 ml min^{-1} was simulated in the 22.6 mm diameter cell. A simulation of the flow field was saved every five time steps.

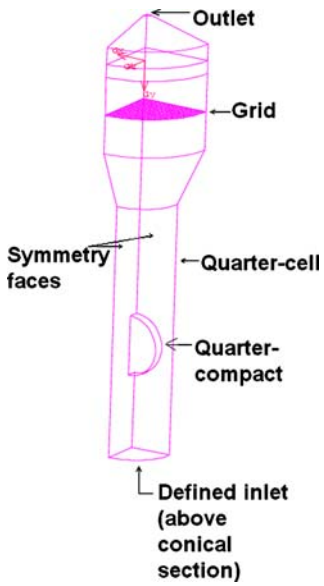

Fig. 1. Diagram illustrating the quarter-cell and quarter-tablet constructed and used in the CFD simulation of hydrodynamics in the 12 mm diameter cell.

Simulation of Species Transfer

As outlined in the introduction section, the second aim of the current work was to simulate the effect of the pulsing flow on the solute concentration gradient at the surface of the dissolving compact. This simulation was designed to complement the flow visualisation studies, where the effect of the pulsing flow near the surface could also be witnessed from the pink colour of the phenolphthalein released as the compact dissolved. The compact used in the flow visualisation studies contained 93% salicylic acid. In order to simulate the effect of "species transfer," that is, in this case, the movement of salicylic acid (i.e. the movement of drug) from the dissolving surface of the compact used in the flow-visualisation studies into the simulated flow field, all surfaces of the compact were defined as being a constant source of salicylic acid. The mass fraction of salicylic acid at the surface was defined as the saturated solubility of salicylic acid in 0.02 M NaOH. The diffusion coefficient of salicylic acid, determined using the method described in the "Experimental Methods" section, was used in the simulation of salicylic acid diffusing from the surface into the medium. As the species transfer simulations involve a second process (that of mass transfer rather than hydrodynamics alone), the mesh was further refined in the

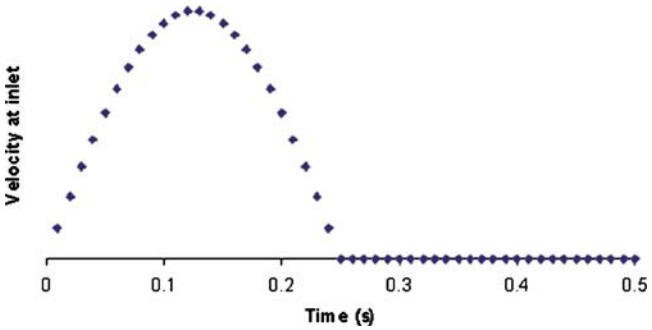

Fig. 2. Velocity magnitude at the inlet *vs.* time (s) over the course of the pulse, illustrating the shape of the flow profile, used as an input to the CFD model to simulate the pulsing flow in the flow-through apparatus.

region of the compact for the purposes of the species transfer simulation, and the time-step reduced to 0.001 s. In order to have a meaningful simulation of the mass fraction of the dissolving species within the cell, and in the region of the compact, it was necessary to simulate species transfer over several pulses (five in total) within the apparatus. This simulation was conducted from the beginning, simultaneously solving for velocity and species transfer. Initially, for the first 1500 time-steps, an approximate solution was obtained, with only 20 iterations per time-step, to allow "build-up" of salicylic acid in the region of the compact surface. After this period, 1000 time-steps (2 pulses, 1 s) were simulated using 100 iterations per time-step. This resulted in residual values of estimated parameters such as velocity and salicylic acid concentration of between approximately 4×10^{-5} and 1×10^{-16} at the end of each time-step. The default residual value in Fluent™ to determine convergence of velocity in x, y and z directions, and of the continuity equation, is 1×10^{-3}. There was little difference in parameter values over the course of consecutive pulses, with the exception of the constantly increasing salicylic acid concentration.

Experimental Methods

Flow Visualisation Studies

A compact of approximately 3.25 mm in height was compressed using an 8.5 mm diameter punch and die set and a Perkin-Elmer hydraulic press. The flow visualisation studies were performed using a modified version of the method used by Mauger *et al.* (28), using a tripod-mounted Canon MV890 digital video camcorder. It should be noted that, as this was a qualitative observational flow visualisation study, no optical distortion reduction methods were used. The compact contained 7% w/v phenolphthalein and 93% w/v salicylic acid (Sigma-Aldrich). The dissolution medium consisted of 0.02 M NaOH (Riedel-de Haën) at 37°C. Flow rates of 5, 17 and 33 ml min^{-1} were used.

A CE 1 flow-through dissolution apparatus and pump (Sotax AG, Switzerland) with a 12 mm diameter cell were used. The conical part of the cell was filled with glass beads of 1 mm diameter. (This operational mode has been termed the "Packed Column"(23).) The compact used in the flow visualisation studies, with the diameter orientated vertically, was placed in a tablet holder in the cylindrical part of the cell.

At the inlet, at the base of the conical part of the cell, is a ruby bead of approximately 5 mm diameter.

Solubility Studies

The solubility of salicylic acid in 0.02 M NaOH at 37°C was determined by adding an excess (1.05 g) of salicylic acid to 50 ml 0.02 M NaOH in a jacketed beaker to maintain a constant temperature, and stirring using a magnetic stirrer. Concentrations were determined by UV spectrophotometry at 295 nm after filtration of samples through a 0.45 μm filter. Samples were taken at 9, 24, 48, 72, 84 h, until the point at which the absorbance did not change significantly (between 72 and 84 h).

Diffusion Coefficient Determination

The diffusion coefficient of salicylic acid in water was determined using the silver membrane filter method, described in detail by Goldberg and Higuchi (29). In brief, it involved measuring the rate of diffusion of the drug across a silver membrane filter. A conical flask (flask I) containing a degassed aqueous solution of salicylic acid (0.01 M) was stirred by a magnetic stirrer. Flask I was modified to incorporate a glass side-arm. A second 250 ml conical flask, also modified to incorporate a glass side-arm, containing distilled water, is the receptor flask (flask II) for the diffusing drug. The side glass side-arms between the flasks are clamped together, and the filter is located at this junction between two Teflon washers. 250 ml of either the salicylic acid solution or water were added to both flasks simultaneously. When the water addition to flask II was completed, flask I was quickly filled to the top, and a glass Y-adapter was placed in position. More salicylic acid solution was added through one of the arms, keeping the stopcock of the other arm open for air displacement. The contents of flask II were sampled at intervals of 30 min, and analysed by U.V. spectrophotometry at 295 nm to determine the diffusion rate of salicylic acid from flask I.

The apparatus was calibrated by measuring the diffusion rate of KCl and comparing the result to the literature value as described by Goldberg and Higuchi (29).

Dissolution Studies

As outlined in the introduction section, the third aim of the current work was to determine the dissolution rate of a vertical planar surface under very low velocity pulsing flow in the flow-through apparatus. In order to interpret the measured dissolution rate, both CFD simulations of the hydrodynamics of this system, as described under "Computational Methods," and experimental dissolution studies under static conditions, or no forced convection, were carried out. Benzoic acid (BA) (BDH - VWR International, Poole, England) 500 mg was compressed into compacts of 13 mm diameter and approximately 3 mm in height using a Perkin Elmer hydraulic press and punch and die set. The compacts were coated with paraffin wax (BDH - VWR International, Poole, England) exposing only one planar surface to the dissolution medium. The coating method involved placing the compact on a glass slide with the planar surface facing

downward. A small amount of molten paraffin wax was then put on the compact, and a small cylindrical lid quickly placed over this as a mould. As the wax rapidly hardened, the lid was removed, and the glass slide removed from the planar surface, which then remains exposed for dissolution. The wax was further pared down to result in a coating of approximately 1 mm thickness. Each compact was then examined to ensure integrity of the coating.

Dissolution in the Flow-Through Apparatus

A CE 7 smart dissolution apparatus (Sotax AG, Switzerland) with a 22.6 mm diameter cell and a flow rate of 8 ml min^{-1} was used. The compact was placed in the tablet holder, with the planar surface orientated vertically.

Dissolution in a Free Convection System

The free convection system consisted of a jar with the compact fixed to the inside of the lid, with the exposed planar surface orientated vertically. A diagram of this free convection system is presented in Fig. 3. In order to ensure that the dissolving surface was fully immersed in the medium, a needle was inserted through the lid and excess dissolution medium introduced. The volume of medium in each jar was approximately 124 ml. The sampling procedure involved careful removal of the lid of the jar with the compact attached. A second lid was then placed on the jar, the medium mixed well and sampled. Fresh medium was then introduced to the jar to replace the sampled volume (10 ml). Finally, the compact was carefully replaced in the jar. Samples were taken every 30 min. Previous in-house studies have shown that the dissolution rate from a compact, located at the top of the jar, when samples were taken in the manner described here, was not significantly different from the dissolution rate determined when separate dissolution experiments were set up for each individual time-point, (i.e. eliminating any effect of the sampling process on the dissolution rate).

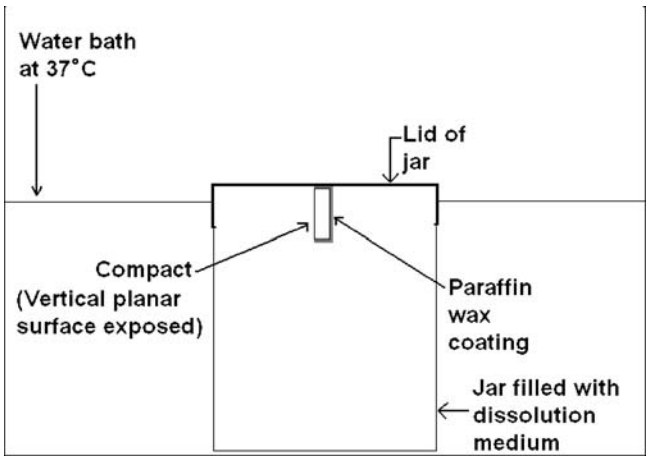

Fig. 3. Diagram depicting the free convection system consisting of the compact (side view) suspended vertically in the jar containing the dissolution medium—only one planar surface of the compact was exposed to the medium with the other surfaces coated with paraffin wax.

All dissolution studies were carried out in triplicate. Dissolution was carried out at 37ºC in 0.1 M HCl. The amount of BA dissolved was determined by UV absorption spectrophotometry at 274 nm.

Prediction of Dissolution Rates

To predict the dissolution rate under natural convection conditions, the following equation correlating with vertical plate mass transfer was used (30):

$$\mathrm{Sh} = 0.673(\mathrm{Ra})^{0.25} \tag{2}$$

where Sh is the dimensionless Sherwood number, defined as $k_L L/D$, L is the length of the active surface, in this case defined as the compact diameter (0.013 m), D is the diffusion coefficient of solute in solvent ($1.236\times10^{-9} m^2 s^{-1}$) and k_L is the mass transfer coefficient. Ra is the Rayleigh number, defined as follows:

$$\mathrm{Ra} = (\nu/\mathrm{D})\left(\left(gL^3\Delta\rho\right)/\left(\nu^2\rho\right)\right) \tag{3}$$

where ν is the kinematic viscosity ($7.043\times10^{-7} m^2 s^{-1}$), g is gravitational acceleration, $\Delta\rho$ is the difference between the density of the saturated solution of the solute in the solvent (1.99 kg m^{-3}) and the density of the pure dissolution medium and ρ is the density of the pure dissolution medium. The methods used to determine these parameters have been previously described (18).

RESULTS

Solubility and Diffusivity

The solubility of salicylic acid in 0.02 M NaOH at 37°C was determined to be 6.4 mg ml^{-1}, and the measured diffusion coefficient of salicylic acid in water was $1.43\times10^{-9} m^2 s^{-1}$.

CFD Hydrodynamic Simulations in the 12 mm Diameter Cell

The velocity vectors shown in Fig. 4 are taken from simulations of flow through the 12 mm diameter cell at 5, 17 and 33 ml min^{-1}. At each flow rate, images are shown from two different time-points over the course of the pulse: As each 0.5 s pulse was divided into 50 time-steps, steps 1–25 represent the half-sine-wave portion of the flow profile, when the fluid is entering the cell (pump discharge). The fastest velocity at this entry point is represented by time-steps 12–13 (0.12–0.13 s). Therefore, hydrodynamics in the cell at the 15th time-step (0.15 s) are representative of the period of high inflow velocity (simulations were saved every 5 time-steps), and the "high inflow velocity" images presented and discussed in this section are taken from simulations at the 0.15 s time-step. The lowest velocity at the entrance is at time-steps 1 and 25. Time-steps 26–50 represent the flat portion of the flow profile, when no liquid is entering the cell (while the pump is drawing fluid from the reservoir). The "zero inflow velocity" images presented and discussed in this section are taken from simulations of the 35th time-step, at 0.35 s. The fluid velocity (represented by vectors coloured by velocity magnitude) around the side of the compact at 5 ml min^{-1} is shown in Fig. 4

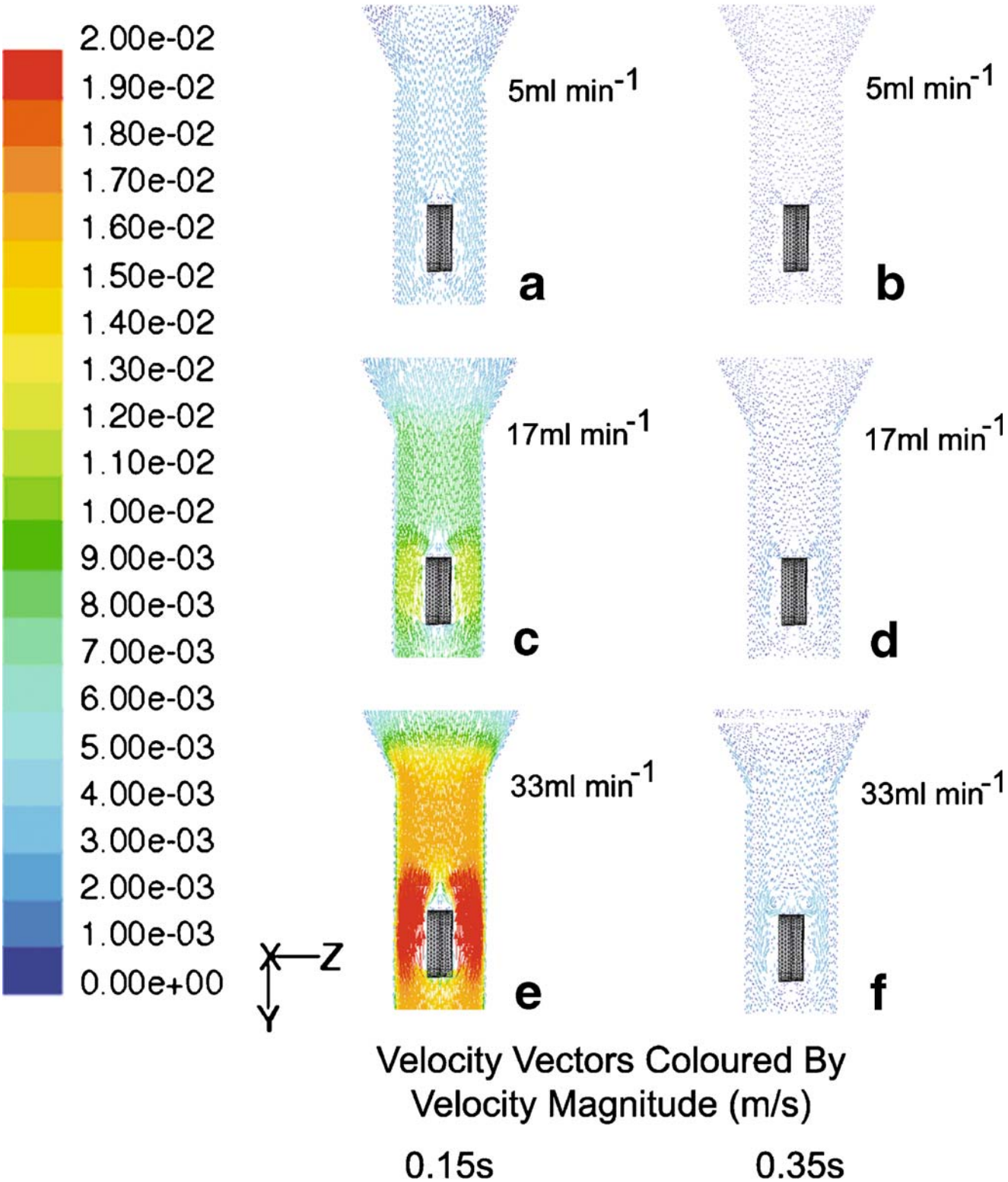

Fig. 4. Vectors coloured by velocity magnitude in the region of the compact in the 12 mm diameter cell, in the flow-through apparatus at a flow rate of 5 ml min^{-1} at high inflow velocity (**a**) and at zero inflow velocity (**b**); at a flow rate of 17 ml min^{-1} at high inflow velocity (**c**) and at zero inflow velocity (**d**); at a flow rate of 33 ml min^{-1} at high inflow velocity (**e**) and at zero inflow velocity (**f**).

(a)–(b), during the "high inflow velocity" period of the flow profile, and during the "zero inflow velocity" period. The velocity profiles around the side of the compact at 17 and 33 ml min^{-1} can be seen in Fig. 4 (c)–(d) and Fig. 4 (e)–(f) respectively. In Fig. 4, (a), (c) and (e) represent the "high inflow velocity" period of the flow profile, and (b), (d) and (f) the "zero inflow velocity" period. The velocity vectors in Fig. 4 illustrate that the magnitude of the variation in hydrodynamics over the

course of a pulse varies with the simulated flow rate. For example, the vectors from Fig. 4 (a) and (b) (5 ml min^{-1}) suggest that although the velocity in the cell is lower at the "zero inflow velocity" point than the "high inflow velocity," the magnitude of the difference in velocities between the two time-points is 0.002–0.004 ms^{-1}. In contrast, the variation between the corresponding time-points at 33 ml min^{-1} is approximately 0.01 ms^{-1}. Additionally, the significance of hydrodynamic variation over the course of the pulse depended on the simulated flow rate. Although the fluid velocity is zero at the inlet during the "zero inflow velocity" period, some circulating motion can be seen above the top of the compact at 17 ml min^{-1}, and this feature is even more prominent at 33 ml min^{-1}. It can be seen that significant fluid movement continues in the cell during the "zero inflow velocity" period, in particular at higher flow rates. Therefore, in Fig. 4, (a), (c) and (e) show an increase in fluid velocity in the cell, as there is a corresponding increase in velocity at the inlet. In contrast, in Fig. 4 (b), (d) and (f), an increase in fluid motion can be observed in the cell from 5 to 17 to 33 ml min^{-1}, despite the fact that there is no increase in inlet velocity at this time-point (0.35 s), as the inlet velocity is zero in each case. The accompanying animation, Animation 1, illustrates the pulsing flow through the 12 mm diameter cell at 17 ml min^{-1} with vectors coloured by velocity magnitude changing over the course of the pulse. The model consists of one quarter of the cell and one quarter of a disk of the same dimensions as the compact used in the flow visualisation studies. The circulating motion over the top of the compact can be seen towards the end of the pulse.

Experimental Flow Visualisation Studies

Visualisation is achieved through dissolution of the salicylic acid and concurrent release of phenolphthalein into the alkaline medium. Images from the flow visualisation experiments at 5, 17 and 33 ml min^{-1} can be seen in Fig. 5 (a)–(b), (c)–(d) and (e)–(f), respectively. It is also possible to observe the pulsing nature of the flow through the cell, particularly at 17 and 33 ml min^{-1}, through the movement of the pink colour from the phenolphthalein as it dissolves from the compact into the 0.02 M NaOH solution. The pH of the saturated solution of salicylic acid in NaOH was measured as approximately 2.9. Therefore, the phenolphthalein will be evident by the pink colour only in the more dilute regions (higher pH) of salicylic acid in the flow visualisation images. This is considered an appropriate visualisation of flow, as regions showing little or no colour are either far from the compact surface (not the region of interest) or in a consistently low velocity or stagnant region allowing build-up of the solute if present.

The accompanying flow visualisation video also clearly demonstrates the pulsing flow around the compact in the 12 mm diameter cell at 17 ml min^{-1}. Fig. 5 (a), (c) and (e) represent images taken from the first part of the pulse, i.e. during the period of positive inflow velocity, and (b), (d) and (f) represent images taken from the "zero inflow velocity" period of the flow profile. At 5 ml min^{-1}, there is little observable difference in the flow near the compact surface. The pink dye moves outward and upwards, and furthermore some downward flow is evident below the compact. The greater amount of dye visible at this lower flow rate in comparison to the higher flow rates is due to the velocity being insufficient to rapidly sweep the dye away from the compact surface. The low fluid velocities predicted from the CFD simulations in Fig. 4 (a)–(b) during both parts of the flow profile support this observation. In both images Fig. 5 (c) and Fig. 5 (e), the stream of colour moving upward and inward over the top of the compact at 17 and 33 ml min^{-1} can be observed. The rapid fluid movement at the compact sides, moving inward over the top of the compact in the CFD simulations, evident in the images in Fig. 4 (c) and (e), correspond with this observed flow feature. The weaker pink colour evident in Fig. 5 (e) results from the higher velocity present in the cell at 33 ml min^{-1} compared to that in Fig. 5 (c) at 17 ml min^{-1}. The effect of the circulating motion at the top of the compact, as indicated in the CFD simulations in Fig. 4 (d) and (f), is evident from the outward movement of the dye at the top of the compact in Fig. 5 (d) and (f). This is more obvious in Fig. 5 (f) than Fig. 5 (d). In Fig. 5 (d), the effect of the low velocity circulating motion above the top of the compact simulated in Fig. 4 (d) is evident as the colour stream directly above the top of the compact moving slightly downwards and outwards compared to Fig. 5 (c).

CFD Species Transfer Simulations

Although the observations from the flow visualisation studies support the hydrodynamic features simulated using CFD, the flow visualisation studies also involve mass transfer as the visualisation is achieved through dissolution of the salicylic acid and concurrent release of phenolphthalein into the alkaline medium. It was considered relevant, therefore, to simulate the effect of the hydrodynamics over the course of the pulse on mass transfer from the compact surface. The simulated flow rate was 17 ml min^{-1}. The results are presented as concentration profiles in Fig. 6. It should be noted that the upper limit of concentration displayed is a mass fraction of 0.00064, which is approximately 10% of the saturated solubility of salicylic acid in NaOH. Any concentration at or above this value is shown in red. Furthermore, as the concentration profiles are compared to the flow visualisation images in Fig. 5, the pink colour from the phenolphthalein indicator represents the concentration profile, during dissolution of the salicylic acid compact, of the more dilute regions of salicylic acid near the compact surface, as described in the experimental flow visualisation section. The image in Fig. 6 (a) is from the high velocity inflow part of the pulse (0.15 s), and that from Fig. 6 (b) is from the zero velocity inflow (0.35 s). The concentration gradient of salicylic acid from the dissolving surface into the bulk dissolution medium is clearly simulated at the top and sides of the compact. There are two "streams" of concentrated regions above the compact at each side. As there will be a dead space directly above the top of the compact (see Fig. 4 (c)–(d)), the solute will build up to some degree here, and will be swept away towards the edges of the compact as it comes in contact with the fluid flowing upwards past the compact sides. During the low velocity period, these streams of more concentrated fluid can be seen to move slightly outwards and downwards (Fig. 6 (b)). This denser concentrated fluid will be influenced by both gravitational effects during the low velocity period and by boundary layer separation. This is evident from the

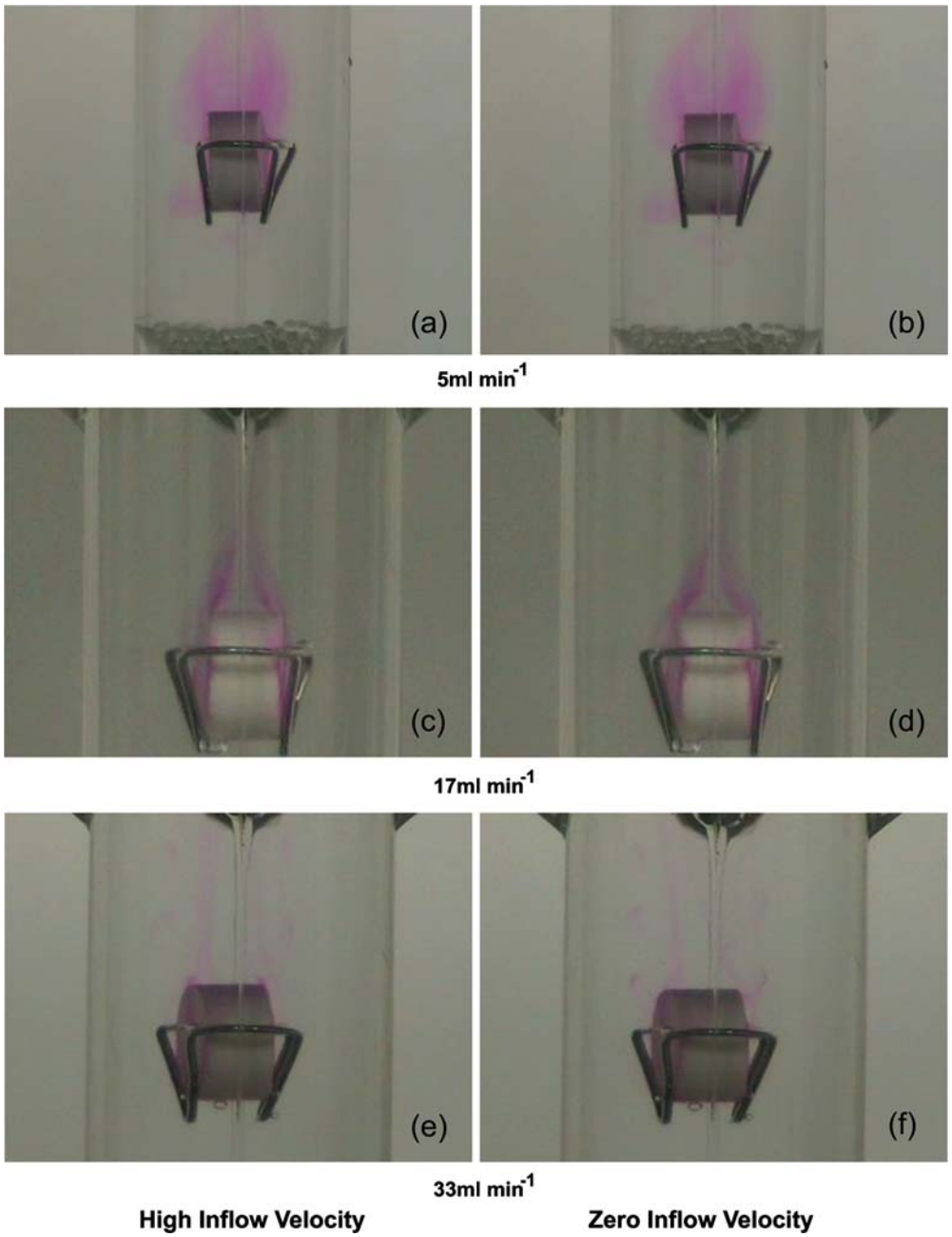

Fig. 5. Flow visualisation revealing flow patterns in the region of the compact in the 12 mm diameter cell, in the flow-through apparatus at a flow rate of 5 ml min^{-1} representing the "high inflow velocity" first part of the pulse (**a**) and the "zero inflow velocity" part of the pulse (**b**); at a flow rate of 17 ml min^{-1} representing the "high inflow velocity" first part of the pulse (**c**) and the "zero inflow velocity" part of the pulse (**d**); at a flow rate of 33 ml min^{-1} representing the "high inflow velocity" first part of the pulse (**e**) and the "zero inflow velocity" part of the pulse (**f**).

circulating fluid at the top of the compact in the CFD image in Fig. 4 (d). The images in Fig. 6 (a) and (b) can be compared to Fig. 5 (c) and (d), respectively. It can be seen that the simulated concentration profiles are in agreement with the observed concentration profiles from the flow visualisation experiments. These simulations can be studied by comparing the accompanying video of flow visualisation at 17 ml min^{-1} with the accompanying Animation 2. Animation 2 is an animation of CFD-generated contours coloured by mass fraction of species (representing salicylic acid proportional concentration) in the 12 mm diameter cell at 17 ml min^{-1} over the course of two pulses. The streams of pink colour from the phenolphthalein transported by the fluid movement around the compact surface can be compared to the simulated regions representing the location of salicylic acid released from the compact in the animation. The simulation is an excellent representation of the experimental flow visualisation result.

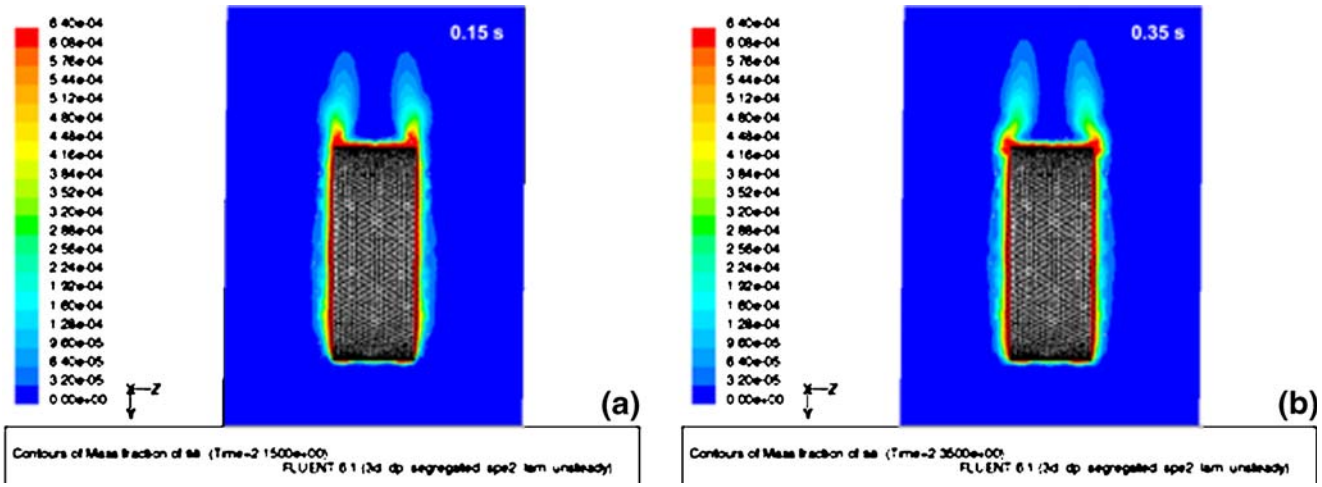

Fig. 6. Concentration profile following simulation of species transfer of salicylic acid into the dissolution medium at 17 ml min^{-1} in the 12 mm diameter cell, at (**a**) high inflow velocity and (**b**) zero inflow velocity.

It is interesting to note the change in concentration near the compact surfaces at both points of the pulse in Fig. 6 (a) and (b). The change in the concentration profile, in terms of relevance to diffusion boundary layer thickness is evident over the course of the pulse, and is also clearly seen in Animation 2. In particular, the thickness is greater at the top and bottom "corners" of the compact during the zero inflow velocity period (0.35 s) than the high inflow velocity period (0.15 s) viewed in Fig. 6. Fig. 7 (a) illustrates the change in diffusion boundary layer thickness at the edges of the planar surface of the compact over 1 s (two pulses). The data is taken from lines created in the flow field, extending from the compact surface into the bulk of the fluid. Line 1 is from the top "corner" (upper end) of the compact, and Line 2 is from the bottom "corner" (lower end); Fig. 7 (b) illustrates the location of these lines. The thickness of the diffusion boundary layer was defined as the distance from the compact surface to the first data point where the concentration is less than 1% of the saturated solubility, i.e. the surface concentration. There will be some minor influence on this calculated distance from the size of the mesh cells; however, it is clear from Fig. 7 that the diffusion boundary layer thickness varies with the pulse at the top and bottom corners of this planar surface. The concentration gradient is generally steeper, represented by a smaller boundary layer thickness during the high inflow velocity period. The thickness then increases during the low inflow velocity period, from 0.25 to 0.5 s and again from 0.75 to 1 s. This change in concentration profile is particularly evident in the animation of the profile over the course of the pulse. As the fluid containing more of the dissolving species will be denser than the bulk medium, the general downward movement of the more concentrated fluid during the low velocity period of the pulse would be expected due to the effect of gravity and resultant natural convection. However, on examination of the velocity vectors presented in Fig. 4, which only contains fluid elements with identical densities as there is no species transfer in the simulation, it is evident that there is outward and downward flow during the low/zero velocity periods of the pulse. This is due to separation of the hydrodynamic boundary layer at the top of the compact as the flow decelerates, and downward flow

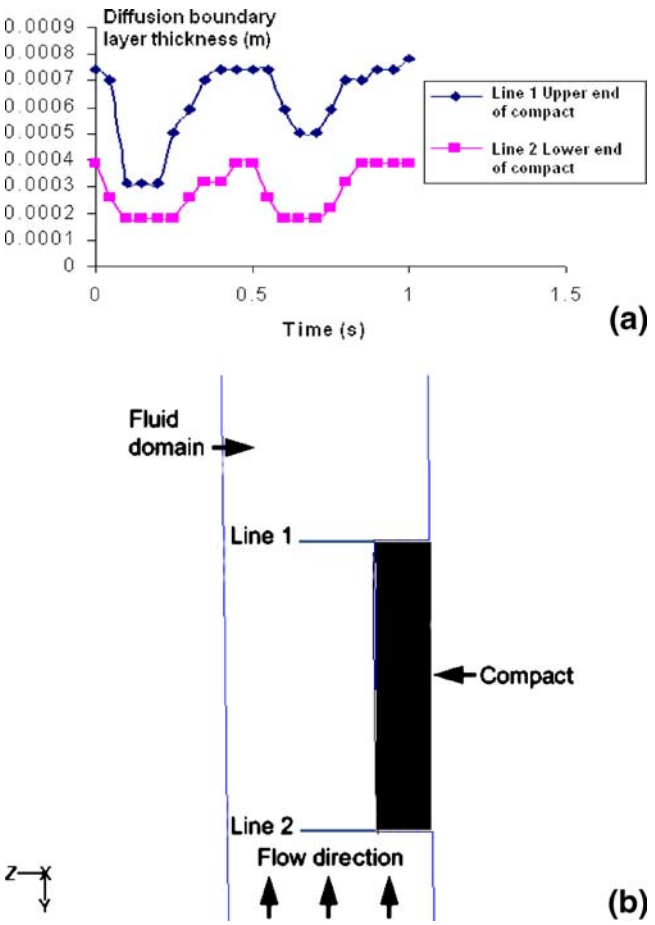

Fig. 7. Graph showing (**a**) the change in diffusion boundary layer thickness over 1 s (2 pulses) at top "corner" of the compact (Line 1 Upper end of compact), and the lower "corner" of the compact (Line 2 Lower end of compact). The location of the profile lines is shown in (**b**). The thickness of the diffusion boundary layer was defined as the distance from the compact surface to the first data point where the concentration is less than 1% of the saturated solubility i.e. the surface concentration.

is evident along the side of the compact and also at the cell wall. This is to be expected due to the adverse pressure gradient experienced by the flow as it moves upwards through the cell but decelerates towards the end of the inflow period (24). Comparison of flow velocities in the region of the compact from the simulations with and without species transfer revealed only minor differences in velocity. In this respect, comparisons are being made between solutions with two different meshes, as the mesh for the species transfer model has been refined near the compact surface. The current results, however, suggest that at the 17 ml min^{-1} flow rate the effect of boundary layer separation dominates over natural convection to cause the downward fluid flow. Regardless of the cause, the changing boundary layer thickness over the course of the pulse impacts on the local dissolution kinetics, in particular at the top and bottom of the vertically orientated compact. The effect of the pulse on the concentration profile from more central locations on the vertical planar surface, away from the top and bottom "corners" was less clear.

Hydrodynamics in the 22.6 mm Diameter Cell and Dissolution Studies

A common operating condition in the larger cell (22.6 mm diameter) is 8 ml min^{-1}. These flow conditions result in a lower average flow velocity than at 5 ml min^{-1} in the 12 mm diameter cell. As the CFD method used to simulate the hydrodynamics in the 12 mm diameter cell resulted in CFD solutions which were supported by the flow visualisation results, the same approach was employed to simulate the flow in the larger 22.6 mm diameter cell. The simulation results are presented in Fig. 8. Although the vectors presented also demonstrate some flow reversal and boundary layer detachment at this flow rate during the zero inflow velocity period, at 0.35 s (Fig. 8b), similar to that observed at 17 ml min^{-1}, it should be noted from the darker blue colour that the velocities are much lower and closer to those at 5 ml min^{-1}. The vectors have been made larger in Fig. 8 compared to Fig. 4 for clarity. The maximum simulated velocity present in the 22.6 mm diameter cell at 1 mm from the surface of the compact at 8 ml min^{-1} was determined to be 1.3×10^{-3} ms^{-1}. This low velocity can be compared to the average simulated velocities of $2.6–6.7\times10^{-2}$ m s^{-1} at common operating conditions in the basket and paddle apparatuses as outlined in the introduction. Due to the extremely low simulated velocities in the 22.6 mm diameter cell at 8 ml min^{-1}, it was anticipated that natural convection may significantly affect dissolution under these conditions. It was therefore decided to compare dissolution results at this flow rate of 8 ml min^{-1} from the vertical planar surface of a compact in the tablet holder to dissolution in a free convection system. The results are shown in Fig. 9.

The dissolution rate of 0.094 (±0.008) mg $min^{-1}cm^{-2}$ in the flow-through cell was found to be lower than that in the free convection system, which was 0.123 (±0.003) mg min^{-1} cm^{-2}. The predicted dissolution rate under natural convection conditions (Eq. 2) was 0.147 mg $min^{-1}cm^{-2}$. This verifies that the dissolution rate measured under natural convection conditions is of the expected magnitude. The dissolution result from the flow-through apparatus suggests that the flow regime in the apparatus may to some extent inhibit dissolution at this very low flow rate.

DISCUSSION

The design of *in vivo* relevant, or biorelevant, dissolution testing necessitates the identification of *in vitro* conditions which are relevant to *in vivo* dissolution. The characterisation

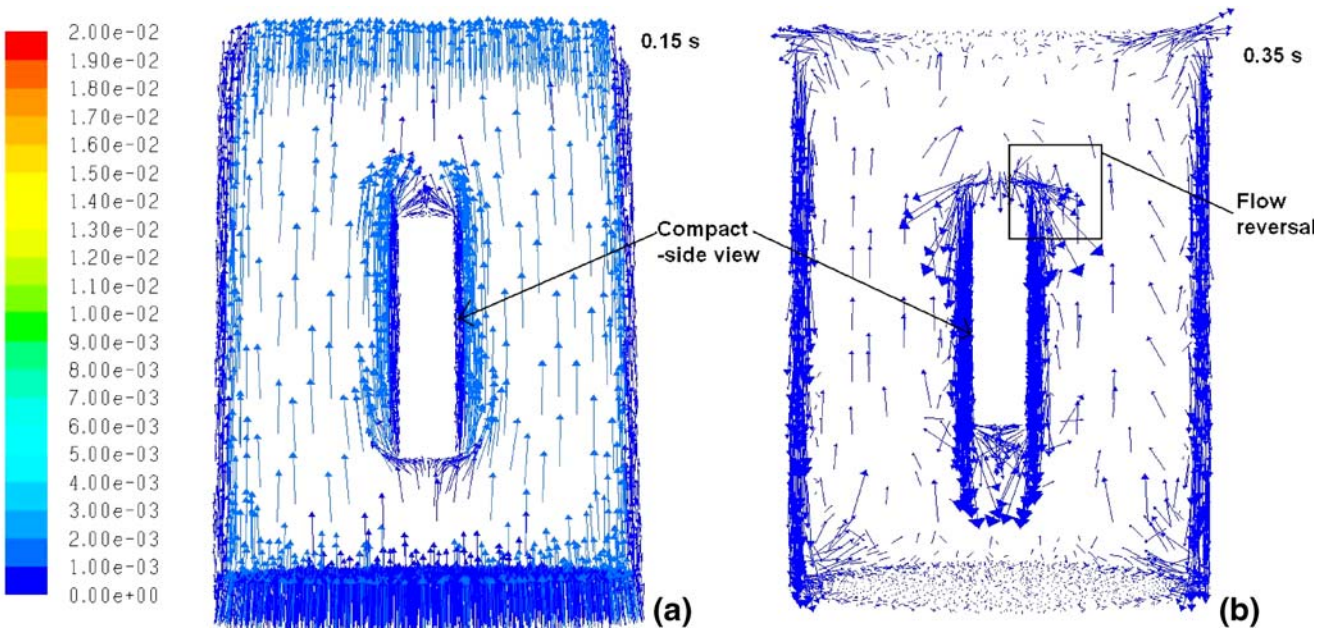

Fig. 8. Vectors coloured by velocity magnitude (ms^{-1}) in the region of the compact in the 22.6 mm diameter cell, in the flow-through apparatus at a flow rate of 8 ml min^{-1} at high inflow velocity (**a**) and at zero inflow velocity (**b**). The vectors near the compact surface in Fig. 8 (b) illustrate the occurrence of some flow reversal and boundary layer detachment.

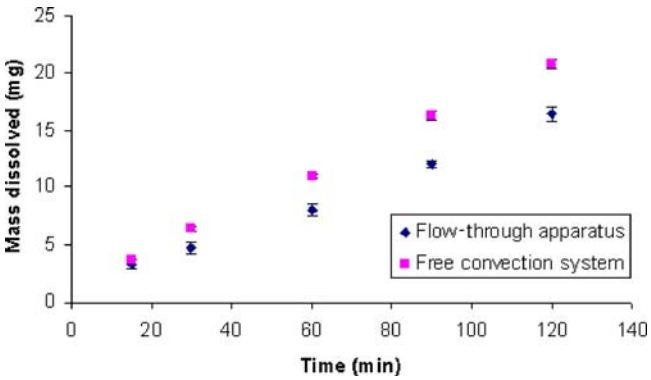

Fig. 9. Mass benzoic acid dissolved (mg) *vs.* time (min) in the flow-through apparatus, 22.6 mm diameter cell at 8 ml min^{-1} and the free convection system.

and development of biorelevant dissolution media has been the subject of a considerable amount of research and investigation (31); however, biorelevant agitation conditions have not been clearly defined. It has been suggested recently that use of lower agitation conditions in the paddle and basket apparatuses may generate fluid velocities which are more relevant, for immediate release (IR) dosage forms, to those fluid velocities encountered *in vivo* (32). This was concluded through comparison of CFD determined fluid velocities in apparatuses used in *in vitro in vivo correlations (IVIVCs).* Furthermore, literature data on physiological gastric slow-wave velocities (33) and CFD simulations of fluid velocities in the stomach (34) were comparable to these slower biorelevant *in vitro* dissolution velocities. In terms of extended (ER) or slow release dosage forms, for example, those based on hydrophilic matrices, intermittent pressure and shear forces experienced during gastro-intestinal transit, have been identified as relevant factors (35). As outlined in the introduction section, maximum fluid velocities in the flow-through apparatus at standard operating conditions are expected to be considerably lower than those found in the paddle or basket apparatuses. As the flow-through apparatus has been used for *in vitro in vivo* correlations (2,4), the current work emphasised the need for insight into the low velocity forced convection flow field in interpreting dissolution test results. Although the low simulated velocities in the 22.6 mm diameter cell at 8 ml min^{-1} would suggest a low dissolution rate, the result obtained, where the dissolution rate was lower than that in the free convection system, suggests that the velocity field present actually inhibits dissolution. This finding, together with the species transfer simulation in the higher velocity flow field of 17 ml min^{-1} in the 12 mm diameter cell (Animation 2), illustrates how dissolution in the cell will be influenced by both the constantly changing flow field over the course of the pulse and the velocities generated by the flow rate used. Dissolution studies in the free convection system are difficult to carry out with respect to repeatability and variability, due to the effects of vibration and background noise. Despite the difficulties in achieving a true "free convection" environment, it might be anticipated that a forced convection system would lead to a higher dissolution rate than a natural convection system.

The fluid flowing through the cell of the flow-through apparatus must flow in an overall upward direction during the half-sine-wave part of the flow profile due to the forced movement induced by the pump. However, the upward flow in a region where significant natural convection is occurring may not have sufficient momentum to overcome the natural downward convection. The impact of natural convection in a low-velocity flow field in a flow-through system has previously been highlighted, with the effect increasing, as expected, with increasing solubility of the solute (5). The current work presents simulations of hydrodynamics over the course of the whole pulse and, therefore, further insight into the potential for natural convection to influence dissolution rates in the compendial flow-through dissolution apparatus. At low flow rates, it is possible that natural convection will influence the hydrodynamics and the dissolution rate to an appreciable extent. On the other hand, at higher flow rates, the impact of natural convection on the overall flow field is more difficult to predict. Although the flow profile at the inlet consists of the half-sine-wave portion and the zero-inflow portion regardless of the flow rate, as can be seen in Fig. 4 (c)–(f) and Fig. 5 (c)–(f), there is significant motion around the compact even during the flat "zero inflow velocity" part of the flow profile, where the dissolution medium is being drawn from the reservoir into the pump. Density gradients at a dissolving surface will exist; however, the effect of gravity on the fluid regions containing these density gradients will be affected by the residual fluid motion in the cell over all parts of the flow profile. In particular, the effect of boundary layer separation and flow reversal near the dissolving compact wall will interact with and possibly dominate over any natural convection effects. As diffusion-controlled dissolution is essentially driven by a concentration gradient, the relative effect of hydrodynamics on the concentration gradient can be inferred from the relationship between fluid velocity near a dissolving surface and dissolution rate, unless the dissolving surface is in an area of low to zero velocity (18). From the current work, it is evident that knowledge of the bulk forced convection component of the system hydrodynamics at 8 ml min^{-1} in the flow-through apparatus is not, by itself, adequate to interpret the effect of the system hydrodynamics on dissolution rate. Rather, it can be used, along with the dissolution rate in the free convection system, to identify flow regimes where the interaction between natural convection, forced convection and boundary layer separation result in a system which does not increase the dissolution rate above that achieved in free convection conditions. The complexity of the effect of the pulsing flow on time-variant concentration gradients, evident from Fig. 7 (a) and (b) and Animation 2, suggests that at low velocities in the flow-through cell, consideration should be given to simulating both local hydrodynamics and species transfer in order to characterise the dissolution conditions.

The results of the hydrodynamics simulations alone are useful in comparing the flow fields within the flow-through apparatus at several flow rates to those in the more commonly used compendial apparatuses, the basket and paddle apparatuses.

From the solution at 0.15 s of the 17 ml min^{-1} flow rate, shown in Fig. 4 (c), there is a maximum simulated facet velocity value at 1 mm from the side of the compact of approximately $1.4\times10^{-2}ms^{-1}$. This can be compared to the maximum simulated velocity at 1 mm from the top and side of a centrally-positioned compact of 13 mm diameter and 3 mm height in the paddle apparatus at 50 rpm of $4.9\times10^{-2}ms^{-1}$ and $6.7\times10^{-2}ms^{-1}$, respectively (20). Therefore, the simulated maximum velocity in the 12 mm diameter cell at 17 ml min^{-1} at 1 mm from the

compact surface is significantly less than that at 1 mm from a compact positioned in the low-velocity area at base of the paddle apparatus. This should be considered in the context of recommended agitation rates of 50–75 rpm in the paddle apparatus (12) and 4–16 ml min^{-1} in the flow-through apparatus (11).

A point to note with respect to the current methodology is that of computational expense *versus* available computational resources, in terms of time and computing power. The approach presented here focussed initially on simulating velocity magnitudes and flow patterns within the flow-through apparatus. In order to gain some insight into the apparatus hydrodynamics over the course of the whole pulse at several flow rates within a realistic time-frame, time-steps of 0.01 s were used, compared to time-steps of 0.00025 s by Kakhi (24). Additionally, the current work simulated flow through the region of interest—the cylindrical portion of the cell only. The results are supported qualitatively by the flow visualisation results presented; however, it is interesting to note how the results compare to the more comprehensive detailed method employed by Kakhi (24). The tangential (vertical) velocity value presented at a flow rate of 16 ml min^{-1} by Kakhi (24), using an equation of the same form to describe the flow profile as that presented in the current work, at the time-point of maximum inflow velocity, was approximately $2.6\times10^{-3} ms^{-1}$ at 0.8 mm from the curved compact surface. Although the shape of the compact in the work by Kakhi is slightly different from that simulated in the current work, the overall velocity values within the cell would be expected to be similar. The value of $2.6\times10^{-3} ms^{-1}$ at twice the flow rate used in the current work (16 ml min^{-1} *vs.* 8 ml min^{-1}) is close to twice the corresponding average vertical velocity value, at the time-point of the simulated maximum inflow velocity, of $1.26\times10^{-3} ms^{-1}$ at 1 mm from the planar surface of the compact in the current work. This confirms that both simulation approaches yield comparable results in terms of overall velocity magnitudes within the cell over the time course of the pulse in the region of interest. The simulation in the current work incorporating species transfer naturally takes longer, not only due to the refined mesh and smaller time-step, but also due to the extra equations which need to be solved to simulate the species transfer superimposed on the hydrodynamic simulation. Although the time scale involved in attaining an informative solution was shorter than that required by Kakhi (24), it still represents a considerable computational expense, as generally initial simulations are carried out using varying solver parameters in order to establish optimal solution and convergence approaches. Therefore, identification of the minimum computation required to identify significant features of interest is vital if simulations of a range of flow conditions are to be considered. Simulations can then be further refined and studied as necessary as was done in the species transfer simulation in the current work. The flow profile generated by the velocity inflow equation used in the current work has been shown to match the actual flow profile metered during discharge from the piston pump (23), and the simulated hydrodynamic features are qualitatively supported by the flow visualisation results. As dissolution testing is a process subject to multiple sources of variability, a CFD simulation can only be used as a tool to aid in interpretation of the observed dissolution process in the physical system of interest. The CFD simulations are presented in the current work as such a tool, with the physical system of interest in this case being low velocity pulsing flow in the flow-through apparatus. Velocimetric techniques, such as particle imaging velocimetry, should be considered if experimental quantitation of a flow field is required.

CONCLUSIONS

CFD can be used to generate simulations of hydrodynamics over the course of the whole pulse within both the 12 and 22.6 mm diameter cells of the flow-through apparatus for a range of flow rates. Flow visualisation techniques can be used to qualitatively validate the hydrodynamic simulation data. Overall, simulated flow velocities at all flow rates investigated are lower than maximum simulated velocities present in the low velocity region of the paddle apparatus, relative to a 13 mm diameter compact at the centre of the vessel base. The simulation of species transfer, which added further qualitative affirmation to the CFD solutions, resulted in a simulated concentration gradient at the dissolving surface. The gradient varied notably over the course of the pulse at the upper and lower edges of the compact. This variation in concentration gradient was thought to be predominantly caused by the flow reversal within the boundary layer, evident from the simulations, although it may also have been influenced by natural convection. The dissolution rate in the flow-through apparatus at 8 ml min^{-1} in the 22.6 mm diameter cell, which was slower than the dissolution rate in a free convection system, may have been influenced by boundary layer separation at the compact surface. This was evident in the CFD simulations of the 22.6 mm cell at this flow rate; however, it is possible that natural convection also influenced local hydrodynamics in the 22.6 mm diameter cell due to the very low velocities present overall. Work is ongoing to investigate the interaction between natural and forced convection in these low velocity conditions. It can be concluded that, accounting for solubility of the solute in question, flow regimes in the flow-through apparatus may result in dissolution rates that are not greater than those in a free convection system and may to some extent inhibit dissolution. This does not imply that these flow conditions are not recommended for pharmaceutical dissolution testing, as in the *in vivo* environment a dosage form is subject to varying, (frequently low) velocity magnitudes and flow directions, including retropulsive flow (32).

In order to fully characterise the flow relevant to a dissolving dosage form, it is recommended that both hydrodynamic and species transfer simulations be considered, particularly at very low flow rates.

As the flow-through apparatus has been used for a diverse range of purposes, including *in vitro in vivo* correlations (2,4) and bioavailability/permeability screening approaches (36,37), in addition to determining the effect of flow rate and hydrodynamics on drug dissolution/release, insight into the hydrodynamics in the flow-through dissolution cell using the methods described here should aid interpretation of dissolution data from the flow-through apparatus.

ACKNOWLEDGEMENTS

The authors would like to acknowledge Richard O'Dwyer for his assistance with the flow-visualisation work.

REFERENCES

1. Butler WCG, Bateman SR. A flow-through dissolution method for a two component drug formulation where the actives have markedly differing solubility properties. Int J Pharm. 1998;173:211–9.
2. Phillips JG, Chen Y, Wakeling IN. A flow-through dissolution approach to *in vivo/in vitro* correlation of adinazolam release from sustained release formulations. Drug Dev Ind Pharm. 1989;15:2177–95.
3. Wu Y, Ghaly ES. Effect of hydrodynamic environment on tablet dissolution using flow-through dissolution apparatus. Puerto Rico Health Sciences Journal. 2006;25:75–83.
4. Sunesen VH, Pedersen BL, Kristensen HG, Müllertz A. *In vivo in vitro* correlations for a poorly soluble drug, danazol, using the flow-through dissolution method with biorelevant dissolution media. Eur J Pharm Sci. 2005;24:305–13.
5. Stevens LE, Missel PJ. Impact of density gradients on flow-through dissolution in a cylindrical flow cell. Pharm Dev Technol. 2006;11:529–34.
6. Zhang GH, Vadino WA, Yang TT, Cho WP, Chaudry IA. Evaluation of the flow-through cell dissolution apparatus: effects of flow rate, glass beads and tablet position on drug release from different type of tablets. Drug Dev Ind Pharm. 1994;20:2063–78.
7. Graffner C, Särkelä M, Gjellan K, Nork G. Use of statistical experimental design in the further development of a discriminating *in vitro* release test for ethyl cellulose ER-coated spheres of remoxipride. Eur J Pharm Sci. 1996;4:73–83.
8. Cammarn SR, Sakr A. Predicting dissolution via hydrodynamics: salicylic acid tablets in flow through cell dissolution. Int J Pharm. 2000;201:199–209.
9. Bhattachar SN, Wesley JA, Fioritto A, Martin PJ, Babu SR. Dissolution testing of a poorly soluble compound using the flow-through cell dissolution apparatus. Int J Pharm. 2002;236:135–43.
10. Hurtado y de la Peña M, Vargas Alvarado Y, Domínguez-Ramírez AM, Cortés Arroyo AR. Comparison of dissolution profiles for albendazole tablets using USP apparatus 2 and 4. Drug Dev Ind Pharm. 2003;29:777–84.
11. United States Pharmacopeia 32, United States Pharmacopeial Convention, Rockwell, MD, USA; 2009.
12. Guidance for industry: Dissolution testing of immediate release solid oral dosage forms, Centre for Drug Evaluation and Reseach, Food and Drug Administration,U.S. Department of Health and Human Services; 1997.
13. Guidance for Industry: Bioavailability and bioequivalence studies for orally administered drug products—General considerations, Center for Drug Evaluation and Research, Food and Drug Administration, U.S. Department of Health and Human Services; 2003.
14. McCarthy LG, Kosiol C, Healy AM, Bradley G, Sexton JC, Corrigan OI. Simulating the hydrodynamic conditions in the United States Pharmacopeia paddle dissolution apparatus. AAPS PharmSciTech 2003; Vol. 4 Article 22.
15. McCarthy LG, Bradley G, Sexton JC, Corrigan OI, Healy AM. Computational fluid dynamics modeling of the paddle dissolution apparatus: agitation rate, mixing patterns and fluid velocities. AAPS PharmSciTech 2004; Vol. 5 Article 31.
16. Kukura J, Arratia PE, Szalai ES, Muzzio FJ. Engineering tools for understanding the hydrodynamics of dissolution tests. Drug Dev Ind Pharm. 2003;29:231–9.
17. Kukura J, Baxter JL, Muzzio FJ. Shear distribution and variability in the USP apparatus 2 under turbulent conditions. Int J Pharm. 2004;279:9–17.
18. D'Arcy DM, Corrigan OI, Healy AM. Evaluation of hydrodynamics in the basket dissolution apparatus using computational fluid dynamics—dissolution rate implications. Eur J Pharm Sci. 2006;27:259–67.
19. Bai G, Armenante P. Hydrodynamic, mass transfer, and dissolution effects induced by tablet location during dissolution testing. J Pharm Sci 2009;98:1511–31
20. D'Arcy DM, Corrigan OI, Healy AM. Hydrodynamic simulation (computational fluid dynamics) of asymmetrically positioned tablets in the paddle dissolution apparatus: impact on dissolution rate and variability. J Pharm Pharmacol. 2005;57:1243–50.
21. Levich VG. Physicochemical hydrodynamics. Englewood Cliffs, N.J., U.S.A.: Prentice Hall Inc.; 1962.
22. Dokoumetzidis A, Papadopoulou V, Valsami G, Macheras P. Development of a reaction-limited model of dissolution: application to official dissolution tests experiments. Int J Pharm. 2008;355:114–25.
23. Kakhi M. Classification of the flow regimes in the flow-through cell. Eur J Pharm Sci. 2009;37:531–44.
24. Kakhi M. Mathematical modelling of the fluid dynamics in the flow-through cell. Int J Pharm. 2009;376:22–40.
25. Stevens LE, Missel PJ, Weiner AL. Controlled flow-through dissolution methodology: a high-performance system. Pharm Dev Technol. 2008;13:135–53.
26. Schiller C, Frölich C-P, Giessmann T, Siegmund W, Mönnikes H, Hosten N, *et al*. Intestinal fluid volumes and transit of dosage forms as assessed by magnetic resonance imaging. Aliment Pharmacol Ther. 2005;22:971–9.
27. D'Arcy DM, Liu B, O'Dwyer R, Bradley G, Corrigan OI. Dissolution in the flow-through apparatus—use of computational fluid dynamics (CFD) to investigate hydrodynamic effects. AAPS Journal 2008;10 (S2).
28. Mauger J, Ballard J, Brockson R, De S, Gray V, Robinson D. Intrinsic dissolution performance testing of the USP dissolution apparatus 2 (rotating paddle) using modified salicylic acid calibrator tablets: proof of principle. Dissolution Technologies 2003; August:6–15.
29. Goldberg AH, Higuchi WI. Improved method for diffusion coefficient determinations employing the silver membrane filter. J Pharm Sci. 1968;57:1583–5.
30. Patrick MA, Wragg AA, Pargeter DM. Mass transfer by free convection during electrolysis at inclined electrodes. Can J Chem Eng. 1977;55:432–8.
31. Jantratid E, Janssen N, Reppas C, Dressman JB. Dissolution media simulating conditions in the proximal human gastrointestinal tract: an update. Pharm Res. 2008;25:1663–76.
32. D'Arcy DM, Healy AM, Corrigan OI. Towards determining appropriate hydrodynamic conditions for *in vitro in vivo* correlations using computational fluid dynamics. Eur J Pharm Sci. 2009;37:291–9.
33. Bradshaw LA, Irimia A, Sims JA, Gallucci MR, Palmer RL, Richards WO. Biomagnetic characterization of spactiotemporal parameters of the gastric slow wave. Neurogastroenterol Motil. 2006;18:619–31.
34. Pal A, Indireshkumar K, Schwizer W, Abrahamsson B, Fried M, Brasseur JG. Gastric flow and mixing studied using computer simulation. Proc R Soc Lond, B, Biol Sci. 2004;271:2587–94.
35. Garbacz G, Wedemeyer R-S, Nagel S, Giessmann T, Mönnikes H, Wilson CG, *et al*. Irregular absorption profiles observed from diclofenac extended release tablets can be predicted using a dissolution test apparatus that mimics *in vivo* physical stresses. Eur J Pharm Biopharm. 2008;70:421–8.
36. Perng C-Y, Kearney AS, Palepu NR, Smith BR, Azzarano LM. Assessment of oral bioavailability enhancing approaches for SB-247083 using flow-through cell dissolution testing as one of the screens. Int J Pharm. 2003;250:147–56.
37. Motz SA, Schaefer UF, Balbach S, Eichinger T, Lehr C-M. Permeability assessment for solid oral drug formulations based on Caco-2 monolayer in combination with a flow through dissolution cell. Eur J Pharm Biopharm. 2007; 66:286–95.